IL NUOVO CIMENTO Vol. 35 C, N. 1 Gennaio-Febbraio 2012
DOI 10.1393/ncc/i2012-11115-y

Colloquia: LaThuile11

Measurement of W, Z and Top properties with CMS

M. De Gruttola on behalf of the CMS Collaboration

University of Florida, Institute for High Energy Physics and Astrophysics
Department of Physics - Gainesville, FL, USA and
Fermi National Accelerator Laboratory - Batavia IL, USA

(ricevuto il 29 Settembre 2011; pubblicato online il 19 Gennaio 2012)

Summary. — We present several measurements in the domain of electroweak and top physics in proton-proton collisions at the LHC at a centre-of-mass energy of 7 TeV. We use data collected with the CMS experiment during the year 2010, and amounting up to a total integrated luminosity of $36\,\mathrm{pb}^{-1}$. Measurements include total cross section productions, asymmetries, top mass measurements and focus on final states with the presence of charged leptons. The results are compared with theory predictions.

PACS 14.70.Fm – W bosons.
PACS 14.70.Hp – Z bosons.
PACS 14.65.Ha – Top quarks.

1. – Introduction

Electroweak (EWK) and top quark measurements are important benchmark process at hadron colliders: the inclusive Z and W cross section are among the first measurement to be performed at LHC, top-quark processes can now be studied extensively in multi-TeV proton-proton collisions, and we can already provide new insights into parton distribution functions with precision measurement of the lepton charge asymmetry.

CMS can extend these measurements to significantly higher energies then the past measurements with LEP and Tevatron, namely, with pp collisions at a center-of-mass energy of 7 TeV provided by the Large Hadron Collider (LHC). The data were collected in 2010, by the Compact Muon Solenoid (CMS) experiment, and correspond to an integrated luminosity of about $36\,\mathrm{pb}^{-1}$. The scheleton of this article is the following: after a first introduction of the CMS detector, we first present the inclusive Z and W cross section measurement, describing also in detail the lepton and missing energy identification and reconstruction in CMS. We than describe the lepton charge asymmetry using W decay identified events, which is among the most outstanding precision EWK measurement performed with CMS data in 2010. Finally we enter in the great domain of top physics study: we describe the top cross section measurement and properties with

leptons in the final state and the first result obtained by the CMS Collaboration for the measurement of the top quark mass.

2. – The CMS detector

A detailed description of the CMS experiment can be found elsewhere [1]. The central feature of the CMS apparatus is a superconducting solenoid, of 6 m internal diameter, 13 m in length, providing an axial field of 3.8 T. Within the field volume are the silicon pixel and strip tracker, the crystal electromagnetic calorimeter (ECAL) and the brass/scintillator hadron calorimeter (HCAL). Muons are measured in gas-ionization detectors embedded in the steel return yoke of the solenoid. The most relevant sub-detectors for this measurement are the ECAL, the muon system, and the tracking system. The electromagnetic calorimeter consists of nearly 76000 lead tungstate crystals which provide coverage in pseudorapidity $|\eta| < 1.479$ in the barrel region and $1.479 < |\eta| < 3.0$ in two endcap regions. A preshower detector consisting of two planes of silicon sensors interleaved with a total of $3\,X_0$ of lead is located in front of the ECAL endcaps. The ECAL has an ultimate energy resolution of better than 0.5% for unconverted photons with transverse energies above 100 GeV. The electron energy resolution is 3% or better for the range of electron energies relevant for this analysis. Muons are measured in the pseudorapidity range $|\eta| < 2.4$, with detection planes made of three technologies: drift tubes, cathode strip chambers, and resistive plate chambers. Matching the muons to the tracks measured in the silicon tracker results in a transverse momentum resolution of about 2% in the relevant muon p_T range.

CMS uses a right-handed coordinate system, with the origin at the nominal interaction point, the x-axis pointing to the center of the LHC, the y-axis pointing up (perpendicular to the LHC plane), and the z-axis along the anticlockwise-beam direction. The polar angle, θ, is measured from the positive z-axis and the azimuthal angle, ϕ, is measured in the x-y plane. The pseudorapidity is given by $\eta = -\ln(\tan(\theta/2))$.

3. – Electroweak measurement

3˙1. *W and Z production cross section.* – The dominant production mechanism for electroweak gauge bosons W and Z in pp collisions is the weak Drell-Yan production process [2], where a quark and an antiquark annihilate to form a vector boson: the reaction $pp \to W + X$ is dominated by $\bar{u}d \to W^+$ and $\bar{d}u \to W^-$ while the $pp \to Z + X$ is dominated by $\bar{u}u, \bar{d}d \to Z$. We present here a measurement of W and the Z production cross sections and their ratios with the full luminosity recorded by CMS at LHC in 2010 corresponding to $36\,\mathrm{pb}^{-1}$.

3˙1.1. Selection. Events with high-E_T electrons are selected online when they pass an unprescaled L1 trigger filter that requires a coarse-granularity region of the ECAL to have $E_T > 5$ or 8 GeV depending on the run period. They subsequently must pass an unprescaled HLT filter that requires an ECAL cluster with E_T well below the offline E_T threshold of 25 GeV, using the full granularity of the ECAL and E_T measurements corrected using offline calibration [3]. Events with high-p_T muon are selected online by the unprescaled single-muon trigger. The energy threshold at the L1 is 7 GeV. The p_T threshold at the HLT level depends on the run period and has been 9 GeV for the first $7.5\,\mathrm{pb}^{-1}$ of collected data and 15 GeV for the remaining $28.4\,\mathrm{pb}^{-1}$.

$W \to ln$ events are characterized by a prompt, energetic and isolated lepton, and significant missing energy ($\not\!\!E_T$). No cut on $\not\!\!E_T$ is applied. Rather, the $\not\!\!E_T$ is used as the main discriminant variable against backgrounds from QCD events.

The Z boson decays to leptons (electrons or muons) are selected based on two energetic and isolated leptons. The reconstructed di-lepton invariant mass is required to lie within a mass window consistent with the known Z boson mass.

Electrons are identified offline as clusters of ECAL energy deposits matched to tracks from the silicon tracker. The ECAL clusters must fall in the ECAL fiducial volume of $|\eta| < 1.44$ for EB clusters or $1.57 < |\eta| < 2.5$ for EE clusters. We select events with one or two electrons having $E_T > 25\,\text{GeV}$ for the $W \to e\nu$ or the $Z \to ee$ analysis respectively. The electron selection criteria were obtained by optimizing signal and background levels according to simulation-based studies, for more details see [4].

Muons candidates are first reconstructed separately in the central tracker (referred to simply as "tracks") and in the muon detector ("stand-alone muons"). Stand-alone muons are then matched and combined with tracker tracks to form "global muons". Another independent algorithm proceeds from the inner tracker outwards matching muon chambers hits, and produce "tracker muons". We require that global and stand-alone muon candidates must have at least one good muon chamber hit. Tracker muons must match to at least two muon stations. Tracks, global and tracker muons must have more than 10 hits in the inner tracker, of which at least one in the pixel detector, and the impact parameter in the transverse plane, d_{xy}, calculated with respect to the beam spot, must be smaller than 2 mm. More details and studies on muon identification can be found in ref. [5].

$W \to \mu\nu$ candidate events must have a muon candidate in the fiducial volume $|\eta| < 2.1$ with $p_T > 25\,\text{GeV}$. We require the muon to be isolated. For $Z \to \mu\mu$ we require two opposite charge muons with the same identification cuts but with $p_T > 20\,\text{GeV}$. The efficiencies for the isolation and identification cuts are obtained with the "Tag and Probe" [4] technique applied on both data and simulation, and correcting the simulation for the residual efficiency ratio.

3˙1.2. Results. The signal and background yields are obtained by fitting the $\not\!\!E_T$ distribution for $W \to e\nu$ and $W \to \mu\nu$. An accurate $\not\!\!E_T$ measurement is essential for distinguishing a signal from QCD multi-jet production backgrounds. We profit from the application of the particle flow (PF) algorithm [6], which provides superior $\not\!\!E_T$ reconstruction performance. The final plots for the W candidate selection and signal fit are reported in fig. 1. The inclusive $Z \to ll$ yield can be obtained counting the number of selected candidates after subtracting the residual background, correcting for the estimated lepton selection efficiencies. The final plots are reported below in fig. 2. Note that the backgroung is so tiny with the given selection cuts that it is not visible in linear scale.

The largest uncertainty for the cross section measurement comes from the knowledge of the integrated luminosity [7, 8] which amounts to 4%. Besides luminosity, the main source of systematic uncertainty comes from lepton efficiency correction factors obtained from the tag-and-probe method. Table I shows a summary of the systematic uncertainties for the W and Z cross section measurements. For all measurements we present results for electrons and muons combined, assuming lepton universality in W and Z decays.

We measure the following cross sections for inclusive W production:

$$\sigma(pp \to WX) \times \text{BF}(W \to \ell\nu) = 10.31 \pm 0.02(\text{stat.}) \pm 0.09(\text{syst.}) \pm 0.10(\text{th.}) \pm 0.41(\text{lumi.})\,\text{nb}. \tag{1}$$

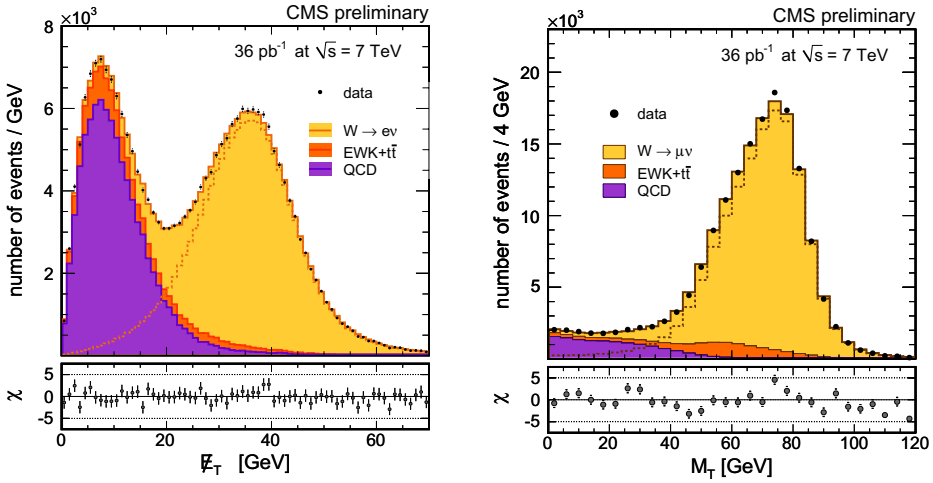

Fig. 1. – (Colour on-line) Left: result of fixed shape template fit on $\not\!\!E_T$ for all $W \to e\nu$ candidates. Right: Total M_T spectrum and fitted contributions for $W \to \mu\nu$ candidate events. Signal from the different processes are shown stacked, W signal (light yellow histogram), other EWK processes (medium orange histogram), and QCD background (dark purple histogram).

The NNLO prediction is 10.44 ± 0.52 nb. The results for charge-specific W production are

$$\sigma(pp \to W^+X) \times \mathrm{BF}(W^+ \to \ell^+\nu) = 6.04 \pm 0.02(\mathrm{stat.}) \pm 0.06(\mathrm{syst.}) \pm 0.08(\mathrm{th.}) \pm 0.24(\mathrm{lumi.})\,\mathrm{nb}; \tag{2}$$

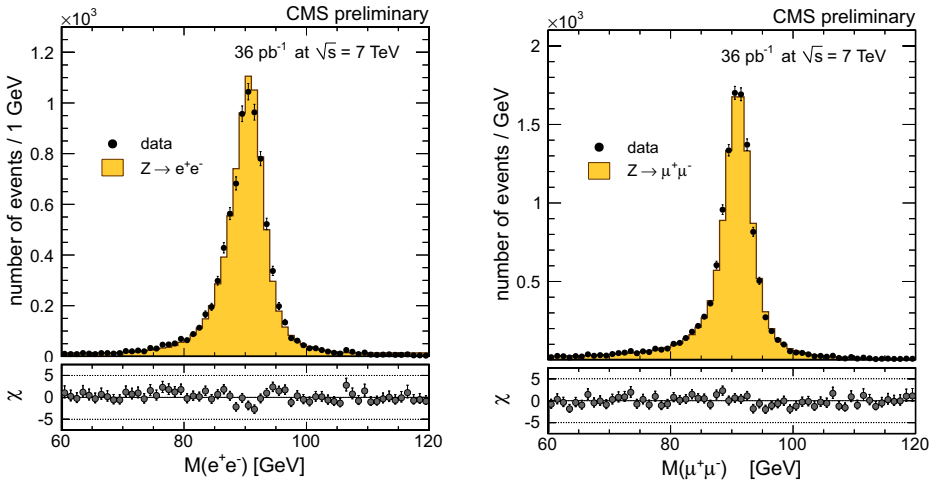

Fig. 2. – Left: $Z \to ee$ signal in linear after applying energy scale correction factors. Right: Distribution of the di-muon invariant mass of $Z \to \mu\mu$ "golden" candidates for data (dots) and for Monte Carlo (histogram) signal and background events.

TABLE I. – *Systematic uncertainties in percent for all inclusive W and Z cross sections. "n/a" means the source does not apply. A common luminosity uncertainty of 4% applies to all channels.*

Source	$W \to e\nu$	$W \to \mu\nu$	$Z \to ee$	$Z \to \mu\mu$
Lepton reconstruction & identification	1.3	0.9	1.8	n/a
Trigger pre-firing	n/a	0.5	n/a	0.5
Momentum scale & resolution	0.5 xspace	0.22	0.12	0.35
$\not\!\!E_T$ scale & resolution	0.3	0.2	n/a	n/a
Background subtraction/modeling	0.35	0.4	0.14	0.28
Trigger changes throughout 2010	n/a	n/a	n/a	0.1
Total experimental	1.5	1.1	1.8	0.7
PDF uncertainty for acceptance	0.6	0.8	0.9	1.1
Other theoretical uncertainties	0.7	0.8	1.4	1.6
Total theoretical	0.9	1.1	1.6	1.9
Total	1.7	1.6	2.4	2.0

and

$$\sigma(pp \to W^- X) \times \mathrm{BF}(W^- \to \ell^- \bar{\nu}) = 4.26 \pm 0.01(\mathrm{stat.}) \pm 0.04(\mathrm{syst.}) \pm 0.07(\mathrm{th.}) \pm 0.17(\mathrm{lumi.})\,\mathrm{nb}. \tag{3}$$

The NNLO predictions for these cross sections are 6.15 ± 0.29 nb for W^+ and 4.29 ± 0.23 nb for W^-. We also measure the following cross sections for Z production:

$$\sigma(pp \to ZX) \times \mathrm{BF}(Z \to \ell^+\ell^-) = 0.975 \pm 0.007(\mathrm{stat.}) \pm 0.007(\mathrm{syst.}) \pm 0.018(\mathrm{th.}) \pm 0.039(\mathrm{lumi.})\,\mathrm{nb}. \tag{4}$$

The reported Z cross sections pertain to the invariant mass range $60 < m_{\ell^+\ell^-} < 120\,\mathrm{GeV}$, and are corrected for the kinematic acceptance but not for γ^* exchange. The NNLO prediction for Z production is 0.97 ± 0.04 nb.

The ratio of cross sections for W and Z production is

$$\frac{\sigma_W}{\sigma_Z} = \frac{N_W}{N_Z}\,\frac{\epsilon_Z}{\epsilon_W}\,\frac{A_Z}{A_W},$$

where A_Z and A_W are the acceptances for Z and W selections, respectively. The uncertainty from A_Z/A_W is determined from Monte Carlo generator studies to be 1.5%. The two different decay channels are combined by assuming fully correlated uncertainty for the acceptance factor, with other uncertainties assumed uncorrelated. This results in the measurements

$$\frac{\sigma(pp \to WX) \times \mathrm{BF}(W \to \ell\nu)}{\sigma(pp \to ZX) \times \mathrm{BF}(Z \to \ell^+\ell^-)} = 10.54 \pm 0.07\,(\mathrm{stat.}) \pm 0.08\,(\mathrm{syst.}) \pm 0.16\,(\mathrm{th.}). \tag{5}$$

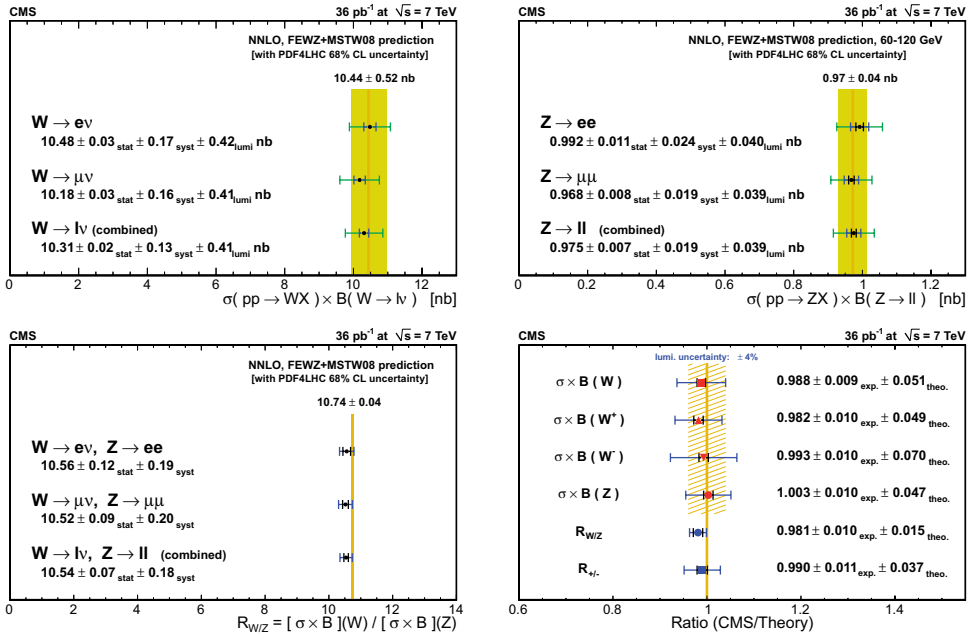

Fig. 3. – Summary of results for W and Z production, W/Z ratio and ratios of CMS measurements to the theoretical values.

The NNLO prediction for this ratio is 10.74 ± 0.04, in good agreement with our measurement. The cross section ratios of W^+ and W^- are given by

$$\frac{\sigma_{W^+}}{\sigma_{W^-}} = \frac{N_{W^+}}{N_{W^-}} \frac{\epsilon_{W^-}}{\epsilon_{W^+}} \frac{A_{W^-}}{A_{W^+}},$$

where A_{W^+} and A_{W^-} are the acceptances for W^+ and W^-, respectively. The uncertainty from A_{W^-}/A_{W^+} is determined from Monte Carlo generator studies to be 2%. The two different decay channels are combined by assuming fully correlated uncertainty for the acceptance factor, with other uncertainties assumed uncorrelated. This results in the measurements

$$\frac{\sigma(pp \to W^+X) \times \mathrm{BF}(W^+ \to \ell^+\nu)}{\sigma(pp \to W^-X) \times \mathrm{BF}(W^- \to \ell^-\bar{\nu})} = 1.421 \pm 0.006(\mathrm{stat.}) \pm 0.014(\mathrm{syst.}) \pm 0.029(\mathrm{th.}). \tag{6}$$

The NNLO prediction is 1.43 ± 0.04, which agrees with the measured values. Summaries of the measurements are given in figs. 3, illustrating the good agreement of our measurements with theoretical predictions computed at the NNLO QCD level with modern NLO PDF sets, as well as the consistency in the measurements in the electron and muon channels. The ratios of our measurements to the theoretical predictions are also reported on the figure.

3˙2. *W asymmetries*. – For lack of space we cannot show all the measurements performed by CMS in 2010 involving W and Z bosons properties. Among all we chose to show a measurement of the lepton charge asymmetry in inclusive $pp \to WX$ production [9]. This high precision measurement of the lepton charge asymmetry, performed in both the $W \to e\nu$ and $W \to \mu\nu$ channels, provides new insights into parton distribution functions. In pp collisions, W bosons are produced primarily via the processes $u\bar{d} \to W^+$ and $d\bar{u} \to W^-$. The first quark is a valence quark from one of the protons, and the second one is a sea antiquark from the other proton. Due to the presence of two valence u quarks in the proton, there is an overall excess of W^+ over W^- bosons. Measurement of this production asymmetry between W^+ and W^- bosons as a function of boson rapidity can provide new insights on the u/d ratio and the sea antiquark densities in in the ranges of the Björken parameter x [10] probed in pp collisions at $\sqrt{s} = 7\,\text{TeV}$. However, due to the presence of neutrinos in leptonic W decays the boson rapidity is not directly accessible. The experimentally accessible quantity is the lepton charge asymmetry, defined to be

$$\mathcal{A}(\eta) = \frac{\mathrm{d}\sigma/\mathrm{d}\eta(W^+ \to \ell^+\nu) - \mathrm{d}\sigma/\mathrm{d}\eta(W^- \to \ell^-\bar{\nu})}{\mathrm{d}\sigma/\mathrm{d}\eta(W^+ \to \ell^+\nu) + \mathrm{d}\sigma/\mathrm{d}\eta(W^- \to \ell^-\bar{\nu})}\,,$$

where ℓ is the daughter charged lepton, η is the charged lepton pseudorapidity, and $\mathrm{d}\sigma/\mathrm{d}\eta$ is the differential cross section for charged leptons from W boson decays. The lepton charge asymmetry can be used to test SM predictions with high precision. Due to the $V-A$ structure of the W boson couplings to fermions, theoretical predictions of the charge asymmetry depend on the transverse momentum (p_T) threshold applied on the daughter leptons. For this reason, we measure $\mathcal{A}(\eta)$ for two different charged lepton p_T (p_T^ℓ) thresholds, 25 GeV and 30 GeV. For this measurement the same lepton identificatuion cuts and trigger described in the previous section has been used, and the same strategy to select W candidates in the onclusive cross section analysis. QCD background is obtained from data using a binned extended maximum likelihood fits performed over the $\not\!\!E_T$ distribution, while the shape for Drell-Yan and other electroweak background are obtained from simulation. Figure 4 shows a comparison of these asymmetries to predictions from the MSTW2008NLO PDF model [11] and the CT10W PDF model [12]. CMS data suggest a flatter pseudorapidity dependence of the asymmetry than the PDF models studied.

4. – The top physics

At the LHC, the $t\bar{t}$ production mechanism is expected to be dominated by a gluon fusion process, whereas at the Tevatron, top-quark pairs are predominantly produced through quark-antiquark annihilation. Measurements of top quark production at the LHC are therefore important new tests of our understanding of the $t\bar{t}$ production mechanism. These measurements are also crucial components in the LHC physics program, since many signatures of new physics models accessible at the LHC either suffer from top-quark production as a significant background or contain top quarks themselves.

4˙1. *Top cross section measurement*. – The cross section for top quark-antiquark pair production has been measured in proton-proton collisions at $\sqrt{s} = 7\,\text{TeV}$ in the data sample corresponding to $36\,\text{pb}^{-1}$ of integrated luminosity collected by the CMS experiment. In the standard model, a top quark decays nearly 100% of the time to a W boson and a b quark. The decay of a $t\bar{t}$ pair is categorized by the decay of the

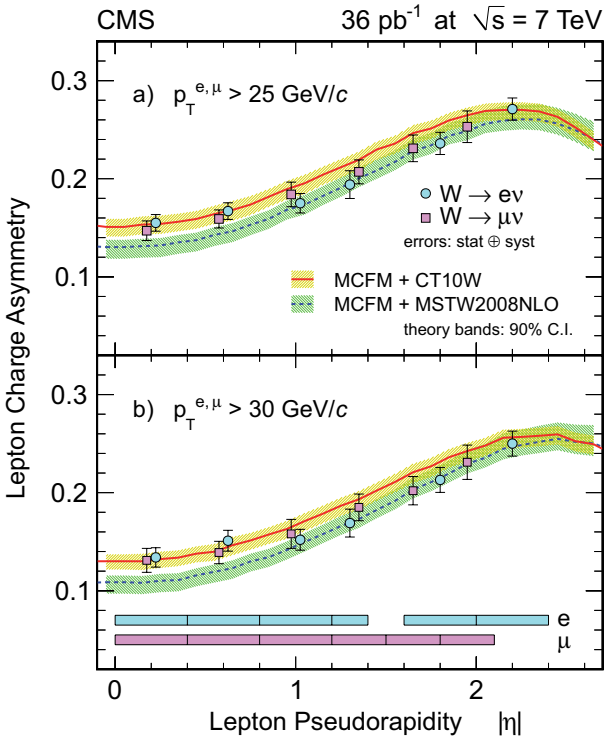

Fig. 4. – Comparison of the measured lepton charge asymmetry to different PDF models for a) lepton $p_T^\ell > 25\,\mathrm{GeV}/c$ and b) lepton $p_T^\ell > 30\,\mathrm{GeV}/c$. The error bars include both statistical and systematic uncertainties. The PDF uncertainty band is corresponding to the 90% confidence interval (CI). The bin width for each data point is shown by the filled bars in fig. b). The data points are placed at the centers of pseudorapidity bins, except that for display purposes the first three data points are shifted +0.025 (−0.025) for electron (muon).

W bosons produced by the pair. Thus the channel in which both W bosons decay to leptons is referred to as the "dilepton" channel, and the channel in which one W decays to leptons and the other to quark jets is the "lepton+jets" channel. The channel in which both W bosons decay to jets is called the "all hadronic" channel. CMS has performed the measurements on both dileptons [13] and leptons+jets sample [14]. Here we report the search in events with two energetic leptons (electrons or muons) in the final state. Presence of the b quark jets in the top-quark decays is tested with a selection requiring jets identified as coming from the b quarks. Results of the measurement in events with and without b quark identification are compared and combined. For semplicity we will only show plots and yields for events without an explicit b-tag requirement. Lepton reconstruction and identification for this analyses are identical to the one descibed before. We rely on single muon and electron trigger. In the event selection for the electron+jets channel, at least one electron with transverse energy greater than 30 GeV and $|\eta|$ less than 2.5 is required, while muons in the muons+jets sample must have $p_T > 20\,\mathrm{GeV}$ and $|\eta| < 2.1$. Selected jets are required to have a jet-energy-scale-corrected $p_T > 30\,\mathrm{GeV}$, $|\eta| < 2.4$, and must be separated by $\Delta R > 0.3$ from isolated electrons and $\Delta R > 0.1$

TABLE II. – *Expected signal and background contributions compared to the number of events observed in data passing full selection with at least two jets and without a b-tagging requirement. Contributions from Drell-Yan and events with non-W/Z leptons are estimated from data and are quoted with statistical and systematic uncertainties combined. All other contributions are estimated from simulation.*

Source	e^+e^-	$\mu^=\mu^-$	$e\mu$
Dilepton $t\bar{t}$	$14.6 \pm 1.2 \pm 2.3$	$18.3 \pm 1.4 \pm 2.8$	$52.5 \pm 3.3 \pm 8.1$
VV	0.3 ± 0.1	0.3 ± 0.1	0.9 ± 0.3
Single top - tW	0.6 ± 0.2	0.7 ± 0.2	1.9 ± 0.6
Drell-Yan τtau	0.6 ± 0.2	0.5 ± 0.2	2.5 ± 0.9
Drell-Yan e^-e^-, $\mu^+\mu^-$	3.0 ± 1.8	7.4 ± 4.1	N/A
Non-W/Z leptons	1.1 ± 1.4	0.6 ± 1.1	1.4 ± 1.6
Total backgrounds	5.5 ± 2.3	9.5 ± 4.3	6.7 ± 2.0
Data	23	28	60

from isolated muons. There is a requirement of $\not\!\!E_T > 30\,\text{GeV}$ for the e^+e^- and $\mu^+\mu^-$ channels, while no $\not\!\!E_T$ requirement for the $e\mu$ sample.

A summary of the expected number of signal and background events is compared with the number of events observed in data in table II for events selected with at least two jets. Good agreement is observed between the expectations and the number of events in data in all channels. The background and signal expectations compared to the number of events in data separately in events with a different jet multiplicity are shown in fig. 5 for events without a b-tagging requirement The $t\bar{t}$ production cross section is measured using

$$\sigma(pp \to t\bar{t}) = \frac{N - B}{AL},$$

where N is the number of observed events; B is the number of estimated background events for data whenever possible; A is the total acceptance relative to all produced $t\bar{t}$ events, including the branching ratio to leptons, the geometric acceptance, and the event selection efficiency already corrected for differences between data and simulation; and L is the integrated luminosity.

The measurements in the three final states (e^+e^-, $\mu^+\mu^-$, $e\mu$) and with and without b-tag requirements can be combined assuming they all correspond to the same physical quantity of the total top-quark pair production cross section. The combination of measurements in all three dilepton final states is found to be

$$168 \pm 18(\text{stat.}) \pm 14(\text{syst.}) \pm 7(\text{lum.})\,\text{pb}. \tag{7}$$

4·2. *Top mass.* – Many methods have been developed for measuring the top quark mass mtop in the dilepton channel. The Matrix Weighting Technique (MWT) [15] has been the first approach, other approaches were also been developed, for example the fully

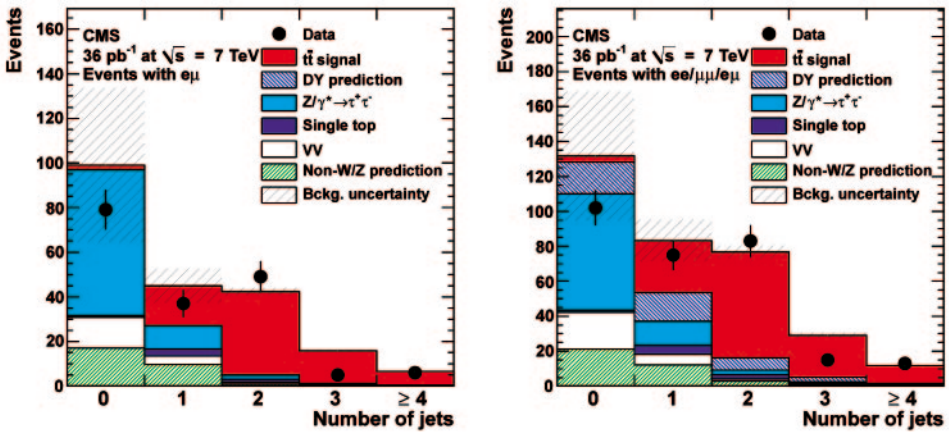

Fig. 5. – Jet multiplicity for events passing full dilepton selection criteria without b-tagging, less the requirement on the number of jets compared to signal expectations from simulation, Drell-Yan and non-W/Z lepton backgrounds estimated in data, and remaining backgrounds estimated from simulation. The total uncertainty on the background contribution is displayed by the shaded area. The distributions are for $e\mu$ and all final-states combined.

kinematic method (KIN) [16]. The average of the measurements in the dilepton channel is $m_{top} = 171.1 \pm 2.5\,\mathrm{GeV}/c$ by Tevatron [17].

The reconstruction of m_{top} from dilepton events leads to an under-constrained system, since the dilepton channel contains at least two neutrinos in the final state. For each $t\bar{t}$ event, the kinematic properties are fully specified by 24 variables, which are the four-

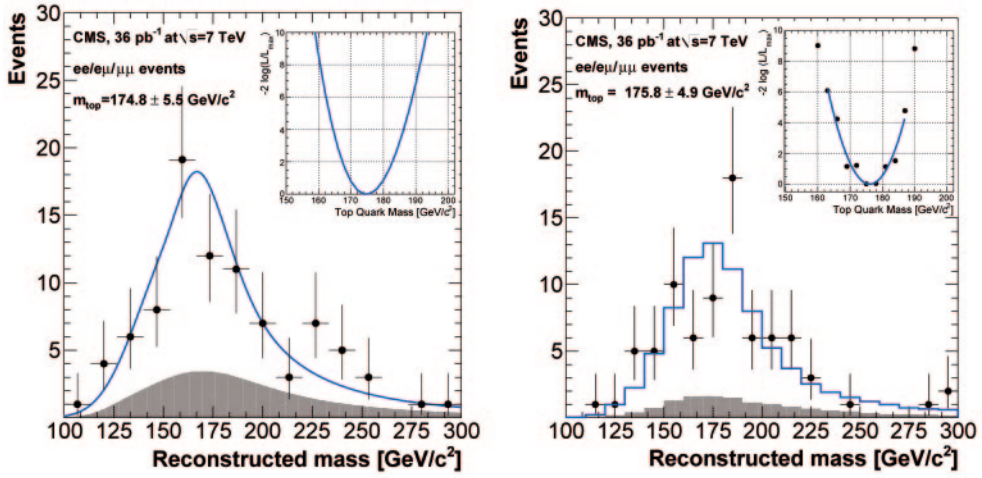

Fig. 6. – Reconstructed mass distribution for the $t\bar{t}$ dilepton events, for the KIN (left) and MWT (right) methods. Also shown is the background shape (shaded) and the sum of background plus MC simulations for $m_{top} = 172.5\,\mathrm{GeV}/c^2$. The inset shows the likelihood fit used to determine the top mass.

momenta of the 6 particles in the final state. Of the 24 free parameters, 23 are known from different sources: 14 are measured (the three-momenta of the jets and leptons, and the two components of the $\not{E}_T$) and 9 are constrained. The system can be constrained by imposing the W boson mass to its measured value (2 constraints), by setting the top and anti-top quark masses to be the same (1), and the masses of the 6 final state particles to the values used in the simulation (6). This still leaves one free parameter that must be constrained by using some hypothesis that depends on the method employed.

A subset of the events selected for measuring the top quark pair production cross section is used to determine m_{top}. In the fully kinematic method KINb, the kinematic equations describing the $t\bar{t}$ system are solved many times per event for each lepton-jet combination. In the analytical matrix weighting technique, the mass of the top quark is used to fully constrain the $t\bar{t}$ system. For a given top quark mass hypothesis, the constraints and the measured observables restrict the transverse momenta of the neutrinos to lie on ellipses in the p_x-p_y plane. If we assume that the measured missing transverse energy is solely due to the neutrinos, the two ellipses constraining the transverse momenta of the neutrinos can be obtained, and the intersections of the ellipses provide the solutions that fulfil the constraints.

The top quark mass is estimated with a likelihood unbinned fit of the experimental mass distribution with the signal and background components, which maximizes the probability that the data are described by a mixture of signal and background events for both the methods. Figure 6 shows the reconstructed top quark mass in the data. The combination of the two measurements yields

$$m_{top} = 175.5 \pm 4.6(\text{stat.}) \pm 4.6(\text{syst.})\,\text{GeV}/c^2. \tag{8}$$

This CMS result is the first measurement of the top quark mas that not performed at the Tevatron.

REFERENCES

[1] CMS Collaboration, *JINST*, **03** (2008) S08004.

[2] Drell S. D. and Yan T. M., *Phys. Rev. Lett.*, **25** (1970) 316, doi:10.1103/PhysRevLett.25.316.

[3] CMS Collaboration, *Electromagnetic calorimeter calibration with* 7 TeV *data*, CMS Physics Analysis Summary CMS-PAS-EGM-10-003 (2010).

[4] CMS Collaboration, *Measurements of Inclusive W and Z Cross Sections in pp Collisions at* $\sqrt{=}7$ TeV, CMS Physics Analysis Summary CMS-PAS-EWK-10-005 (2010).

[5] CMS Collaboration, *Performance of CMS muon identification in pp collisions at* $\sqrt{=}7$ TeV, CMS PAS MUO-2010-002 (2010).

[6] CMS Collaboration, *Particle-flow commissioning with muons and electrons from J/Psi and W events at* 7 TeV, CMS PAS PFT-2010-003 (2010).

[7] CMS Collaboration, *Measurement of CMS luminosity*, CMS PAS EWK-2010-004 (2010).

[8] CMS Collaboration, *Absolute luminosity normalization*, CMS DPS 2011-002 (2011).

[9] CMS Collaboration, *Measurement of the Lepton Charge Asymmetry in Inclusive W Production in pp Collisions at* $\sqrt{s} = 7$ TeV, arXiv:1103.3470v1 [hep-ex] 17 Mar 2011, *JHEP*, **04** (2011) 50.

[10] Bjorken J. D. and Paschos E. A., *Phys. Rev.*, **185** (1969) 1975, doi:10.1103/PhysRev.185.1975.

[11] Martin A. D., Stirling W. J., Thorne R. S. *et al.*, *Eur. Phys. J. C*, **63** (2009) 189, arXiv:0901.0002, doi:10.1140/epjc/s10052-009-1072-5.

[12] Lai H.-L. *et al.*, *Phys. Rev. D*, **82** (2010) 074024, arXiv:1007.2241, doi:10.1103/PhysRevD.82.074024.
[13] CMS Collaboration, *Measurement of the $t\bar{t}$ production cross section and the top quark mass in the dilepton channel in pp collisions at $\sqrt{s} = 7$ TeV*, arXiv:1105.5661v1 [hep-ex] 27 May 2011, *JHEP*, **07** (2011) 49.
[14] CMS Collaboration, *Measurement of the $t\bar{t}$ Production Cross Section in pp Collisions at $\sqrt{s} = 7$ TeV using the Kinematic Properties of Events with Leptons and Jets*, arXiv:1106.0902v1 [hep-ex] 5 June 2011, *Eur. Phys. J. C*, **71** (2011) 1721.
[15] D0 Collaboration, *Phys. Rev. Lett.*, **80** (1998) 2063, arXiv:hep-ex/9706014, doi:10.1103/PhysRevLett.80.2063.
[16] CDF Collaboration, *Phys. Rev. D*, **73** (2006) 112006, arXiv:hep-ex/0602008, doi:10.1103/PhysRevD.73.112006.
[17] CDF and D0 Collaboration, *Combination of CDF and D0 results on the mass of the top quark* (2010) arXiv:1007.3178v1 [hep-ex].